Applied Catalysis B: Environmental 125 (2012) 304–310

Contents lists available at SciVerse ScienceDirect

Applied Catalysis B: Environmental

journal homepage: www.elsevier.com/locate/apcatb

A facile synthesis of nearly monodisperse ruthenium nanoparticles and their catalysis in the hydrolytic dehydrogenation of ammonia borane for chemical hydrogen storage

Hasan Can, Önder Metin*

Department of Chemistry, Faculty of Science, Atatürk University, 25240 Erzurum, Turkey

ARTICLE INFO

Article history:
Received 8 April 2012
Received in revised form 24 May 2012
Accepted 30 May 2012
Available online 7 June 2012

Keywords:
Ruthenium nanoparticles
Al_2O_3 nanopowder
Heterogeneous catalyst
Dehydrogenation
Ammonia borane

ABSTRACT

A facile method for the preparation of nearly monodisperse Ru nanoparticles (NPs) and their record catalytic activity in the hydrolytic dehydrogenation of ammonia borane (AB) for chemical hydrogen storage are reported herein. Ru NPs were prepared by a novel protocol comprising the thermal decomposition and concomitant reduction of ruthenium(III) acetylacetonate ($Ru(acac)_3$) in the presence of oleylamine (OAm) and benzylether (BE). In the protocol, OAm served as both a stabilizer and reducing agent and BE used as a solvent. Ru NPs were supported on aluminum oxide nanopowder ($Ru@Al_2O_3$) via a simple liquid impregnation method before their use as catalyst for the dehydrogenation of AB in water. Without any special treatment to remove the surfactants, $Ru@Al_2O_3$ showed high catalytic activity in the hydrolytic dehydrogenation of AB providing an initial turnover frequency (TOF) of 39.6 mol H_2 (mol Ru min)$^{-1}$. Their catalytic performance was further enhanced dramatically by the acetic acid treatment and the initial TOF value is increased to 83.3 mol H_2 (mol Ru min)$^{-1}$ that is the highest among the reusable Ru catalysts and even higher than Pt-based catalysts tested in the hydrolysis of AB. Additionally, the work reported here includes a wealth of kinetic data to determine the rate law and apparent activation parameters for the catalytic dehydrogenation of AB in water.

1. Introduction

The use of transition metal nanoparticles (NPs) in catalysis has attracted much attention in all areas of science and technology because of its high activity and selectivity associated with their small particle size and large surface area [1–3]. In recent years, Ru NPs have emerged as one of the most active catalysts among other transition metals due to their high activities under mild conditions in various catalytic reactions [4,5]. Many chemical routes have been reported for the preparation of Ru NPs including alcohol reduction [6] or borohydride reduction [7] either in water or organic solvents in the presence of various stabilizers [8–10]. However, monodisperse Ru NPs with shape and size control are only made by decomposition of organometallic Ru complexes in the presence of surfactants such as long-chain thiols [11,12] or polymers [13,14] that bind strongly to surface of Ru, which forms a hindrance to obtain high catalytic activity. Although there are some reports on the removing those type of surfactants from the NPs surface [15], the aggregation of NPs and catalysis deterioration is unavoidable in those protocols. In this regard, the preparation of Ru NPs with a narrow size distribution in the presence of weakly binding surfactants is aspired to develop their highly active heterogeneous catalysts. In our recent study, we demonstrated that monodisperse Ni NPs prepared from the reduction of nickel(II) acetylacetonate by borane ter-butylamine in oleylamine (OAm) and oleic acid as surfactants are highly active and stable catalysts in the hydrolytic dehydrogenation of ammonia borane (AB) [16]. Sun et al. also reported highly active catalysis of monodiperse palladium NPs prepared from reduction palladium(II) acetylacetonate by borane ter-butylamine in OAm for the formic acid oxidation [17]. Correlatively, the preparation of monodiperse Ru NPs in the presence of OAm or oleic acid as a weakly binding surfactant will be advantageous for the preparation of highly active and stable Ru nanocatalyst.

On the other hand, the storage of hydrogen is still a major hurdle for prospective hydrogen economy although the use of hydrogen as an energy carrier in various daily-life applications has been already initiated. Recently, ammonia borane (AB, $H_3N{\cdot}BH_3$) has been regarded as the most promising entrant for vehicular hydrogen storage applications among all other chemical hydrogen storage materials [18–21] owing to its high hydrogen content of 19.6 wt% that is greater than the 2015 target of the U.S. Department of Energy (9 wt% hydrogen for a material) [22] and stability

* Corresponding author. Tel.: +90 442 231 4410; fax: +90 442 236 0948.
E-mail addresses: ometin@atauni.edu.tr, ondermetin1981@hotmail.com (Ö. Metin).

0926-3373/$ – see front matter © 2012 Elsevier B.V. All rights reserved.
http://dx.doi.org/10.1016/j.apcatb.2012.05.048

in the solid state under ambient conditions [23,24]. The hydrogen stored in AB can be released through different ways [25–27], but the hydrolytic dehydrogenation of AB (hydrolysis, Eq. (1)) [28–30] seems to be most promising route considering on-board applications [31].

$$H_3NBH_3(aq) + 2H_2O(l) \rightarrow (NH_4)BO_2(aq) + 3H_2(g) \quad (1)$$

However, a catalyst facilitating the B—N bond cleavage is required to generate hydrogen from the hydrolysis of AB due to the strong B—N bond of AB [32–35]. Because of the advantages of heterogeneous catalysis, current research on finding new catalyst systems that possess high activity with a practical rate of hydrogen generation from the hydrolysis of AB has been directed toward the development of heterogeneous catalysts [36–42].

Herein we report a facile method for the preparation of nearly monodisperse Ru NPs and their superb catalysis in the hydrolytic dehydrogenation of AB under ambient conditions. The Ru NPs were prepared by a facile and novel method comprising the thermal decomposition and concomitant reduction of ruthenium(III) acetylacetonate ($Ru(acac)_3$) in the presence of oleylamine (OAm) and benzylether (BE). In our protocol, OAm served as both a surfactant and reducing agent and BE was used as a solvent. The as-prepared Ru NPs are dispersible and colloidally stable for months in nonpolar solvents such as hexane and tetrahydrofuran. Without any special treatment to remove the surfactants, as-prepared Ru NPs were supported on aluminum oxide nanopowder ($Ru@Al_2O_3$) via simple liquid impregnation method and showed high catalytic activity and stability in the hydrolytic dehydrogenation of AB. Their catalytic performance was further enhanced dramatically by the acetic acid treatment and the TOF value is increased from 39.6 to 83.3 mol H_2 (mol Ru min)$^{-1}$ that is the best among the reusable Ru catalyst and even higher than the best Pt-based catalysts tested in the hydrolysis of AB. Kinetics of the $Ru@Al_2O_3$ catalyzed hydrolytic dehydrogenation of AB was also studied depending on the catalyst concentration, substrate concentration and temperature.

2. Experimental

2.1. Chemicals

All commercially obtained chemicals were used as received unless indicated otherwise. Ruthenium(III) acetylacetonate (99%), oleylamine (OAm, >70%), borane ammonia complex (AB, 97%), hexane (99%), benzyl ether (BE, 97%), aluminum oxide nanopowder (γ-Al_2O_3, particle size <50 nm (TEM), surface area >40 m^2/g (BET)), acetic acid (99%), isopropanol, deuterated water and chloroform were purchased from Sigma–Aldrich®. All glassware and Teflon-coated magnetic stir bars were cleaned with acetone, followed by copious rinsing with distilled water before drying at 150 °C in oven for overnight.

2.2. Instrumentation

Transmission electron microscope (TEM) and high resolution TEM (HRTEM) images were obtained using a JEM-2100 (JEOL) instrument operating at 200 kV. Samples were examined at magnification between 50 and 800 K. X-ray diffraction pattern (XRD) was recorded on a Rigaku Miniflex diffractometer with Cu Kα (30 kV, 15 mA, λ = 1.54051 Å), over a 2θ range from 10° to 80° at room temperature. Ruthenium content of the catalyst samples were determined by using Leiman series inductively coupled plasma-optical emission spectroscopy (ICP-OES) after each sample was completely dissolved in aqua-regia (HNO_3/HCl: 1/3, v/v, ratio). ^{11}B NMR spectrum was measured on a Bruker Avance DPX 400 MHz spectrometer (400.1 MHz for ^1H NMR; 100.6 MHz for ^{13}C NMR; 128.2 MHz for ^{11}B NMR). $BF_3{\cdot}(C_2H_5)_2O$ was used as the external reference for ^{11}B NMR chemical shifts.

2.3. Synthesis of ruthenium nanoparticles and supporting them on nano γ-Al_2O_3

In a typical synthesis, 200.0 mg ruthenium(III) acetylacetonate (0.5 mmol Ru), 10.0 mL of OAm and 8.0 mL of BE were mixed and stirred at 1000 rpm under continuous nitrogen flow in a special four-necked reactor. Owing to jacketed heater and connected thermocouple placed into the reactor, the mixture was heated up to 120 °C slowly and kept at this temperature for 1 h. Next, the resulted solution was heated to 300 °C (20 °C/min) and maintained at this temperature for 1 h. Then, the mixture was cooled down to 40 °C and centrifuged at 8000 rpm for 10 min after the addition of isopropanol into the each nanoparticle solution separated into four centrifuge tubes. After centrifugation, a very few amount of Ru NPs stacked on the surface of centrifuge tubes was discarded and the supernatant solution was transferred into the 250 mL of erlenmayer. Next, 1.5 g of Al_2O_3 nanopowder was added into the supernatant solution and stirred for overnight. The resultant mixture was centrifuged at 6000 rpm for 12 min for the separation of Al_2O_3 nanopowder supported Ru NPs ($Ru@Al_2O_3$). The isolated $Ru@Al_2O_3$ catalyst were redispersed in hexane and centrifuged at 6000 rpm for 12 min again to remove the unsupported Ru NPs. Finally, the $Ru@Al_2O_3$ catalysts were dispersed in water (20 mL) and treated with 640 mg AB before testing their catalytic activity in the hydrolytic dehydrogenation of AB.

2.4. Hydrolytic dehydrogenation of ammonia borane catalyzed by $Ru@Al_2O_3$

A desired amount of as-prepared $Ru@Al_2O_3$ catalysts were dispersed in 7.0 mL of water in the jacketed reactor thermostated at 25.0 ± 0.5 °C. Next, 2.0 mmol AB dissolved in 3.0 mL of water was injected into the catalyst solution via gastight syringe under vigorous stirring and hydrogen gas evolution started immediately. The catalytic hydrolysis reaction was followed by measuring the hydrogen generation with time. Hydrogen gas generation from the catalytic reaction solution was followed by using a typical water-filled gas burette system and recording the displacement of water level in the gas burette every minute until no more hydrogen evolution observed. Next, an approximately 0.1 mL aliquot of the reaction solution in the reactor was withdrawn with a glass Pasteur pipette and added to 0.5 mL of D_2O in a quartz NMR sample tube (Norell S-500-QTZ), which was subsequently sealed. The ^{11}B NMR spectrum of this solution showed the complete conversion of H_3NBH_3 (quartet at −23 ppm) to ammonium metaborate giving a peak at 9.1 ppm.

2.5. Kinetics of hydrolytic dehydrogenation of AB catalyzed $Ru@Al_2O_3$

In order to establish the rate law and obtain the activation parameters for the hydrolytic dehydrogenation of AB catalyzed by $Ru@Al_2O_3$, three different sets of experiment were performed in the same ways described in Section 2.4. In the first set of experiments, the concentration of AB was kept constant at 200.0 mM and the amount of $Ru@Al_2O_3$ catalyst (1 wt% Ru) was varied in the range of 50, 75, 100, 125 and 150 mg at 25 ± 0.5 °C. In the second set of experiments, the amount of $Ru@Al_2O_3$ catalyst (1 wt% Ru) was held constant at 100 mg while AB concentration was varied in the range of 100, 200, 300, 400 and 500 mM at 25 ± 0.5 °C. Finally, the catalytic dehydrogenation of AB was performed at constant AB concentration (200.0 mM) and amount of $Ru@Al_2O_3$ catalyst (75 mg, 1 wt% Ru) at various temperatures in the range of 20–40 °C in order to

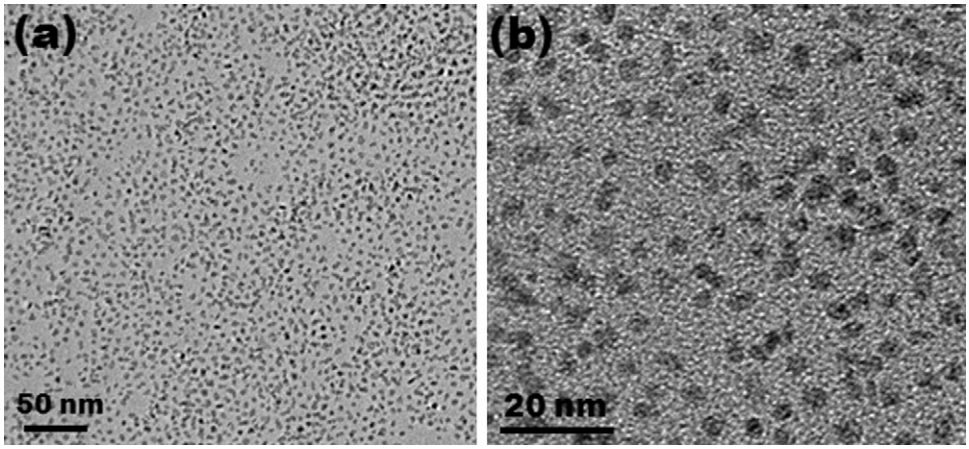

Fig. 1. (a) Low-magnification and (b) high-magnification TEM images of Ru NPs taken from the hexane dispersion.

obtain the apparent activation energy (E_a^{app}). The volume of hydrogen versus time data was processed using Origin 8.0 software.

2.6. Acetic acid treatment of $Ru@Al_2O_3$ catalyst

The $Ru@Al_2O_3$ catalysts were cleaned with acetic acid as reported elsewhere [9]. Briefly, $Ru@Al_2O_3$ (250 mg) catalysts were suspended in 50.0 mL of acetic acid and the suspension was heated to about 70 °C for 10 h. The catalyst was separated by centrifugation and washed with ethanol two times.

2.7. Reusability of $Ru@Al_2O_3$ catalyst in the hydrolysis of AB

In a typical reusability test, $Ru@Al_2O_3$ catalysts were isolated from the catalytic reaction solution by centrifugation at 6000 rpm for 12 min after all of the AB present in solution was consumed for each cycle. The isolated $Ru@Al_2O_3$ catalysts were washed several times with water to remove the residuals from the surface of the catalyst. Next, a new catalytic reaction was started by dispersing the isolated $Ru@Al_2O_3$ catalysts in a solution containing a new batch of 2.0 mmol AB as described in Section 2.4.

3. Results and discussion

3.1. Synthesis and characterization of Ru NPs

Ru NPs were prepared by thermal decomposition and concomitant reduction of ruthenium(III) acetylacetonate in the presence of OAm and benzyl ether. In our protocol, OAm was used as both surfactant and reducing agent and benzyl ether served as a high boiling solvent. Fig. 1 shows the representative TEM images of freshly prepared Ru NPs taken from the hexane dispersion at different magnifications. As clearly seen from the TEM images, Ru NPs have a very narrow size distribution with a mean particle size of 2.5 nm. The particle size of Ru NPs ranges in 2.2 nm and 2.9 nm with a standard deviation of 12%, which reveals a nearly monodisperse size distribution of Ru NPs. However, there are some particles with an irregular shape seen from the TEM image that is indicative of the inhomogeneous nucleation process. The development of the current recipe for the preparation of more uniform Ru NPs and their size control is under investigation in our laboratory.

Powder-XRD and HRTEM analyses were performed on as-prepared Ru NPs to investigate their crystallinity. Fig. 2b shows the XRD pattern of Ru NPs taken from their films formed by evaporation of the hexane dispersion on amorphous glass. One shoulder peak at $2\theta = 38.4^\circ$, one broad peak at $2\theta = 42.9^\circ$ and two small diffuse peaks at $2\theta = 56.1^\circ$ and 69.1° are observed in the XRD pattern which are attributed to (1 0 0), (0 0 2), (1 0 1), (1 0 2) and (1 1 0) planes of hexagonal close packed structure of metallic Ru (JCPDS No. 06-0663), respectively [39]. The broad peak at $2\theta = 42.9^\circ$ emerged most probably due to the very small size of Ru NPs and considered to be the overlapping of two peaks at 42.3° (0 0 2) and 44.1° (1 0 1). A HRTEM study of a series of single Ru NPs indicates that they have a polycrystalline structure (Fig. 2a) but the (1 0 1) planes can still be identified by the typical interfringe distance of 0.216 nm, which is close to the lattice spacing of the (1 0 1) planes of the hexagonal Ru (0.211 nm).

3.2. Preparation and characterization of $Ru@Al_2O_3$

Ru NPs have the hydrophobic surface due to presence of OAm as the surfactant and therefore their use as catalysts for the

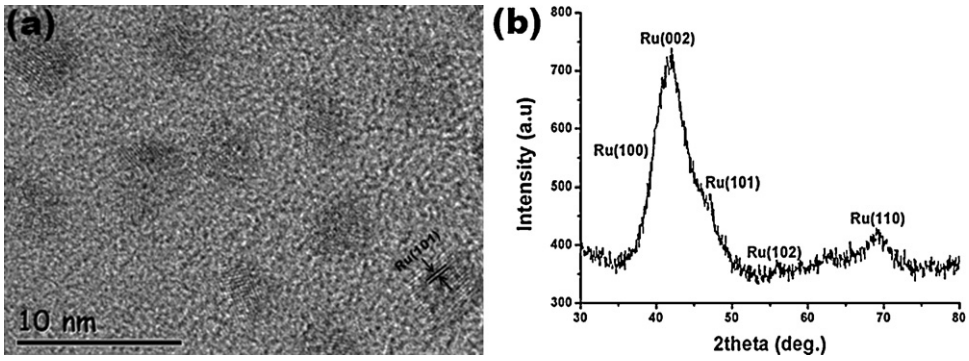

Fig. 2. (a) HRTEM image and (b) XRD pattern of as-prepared Ru NPs.

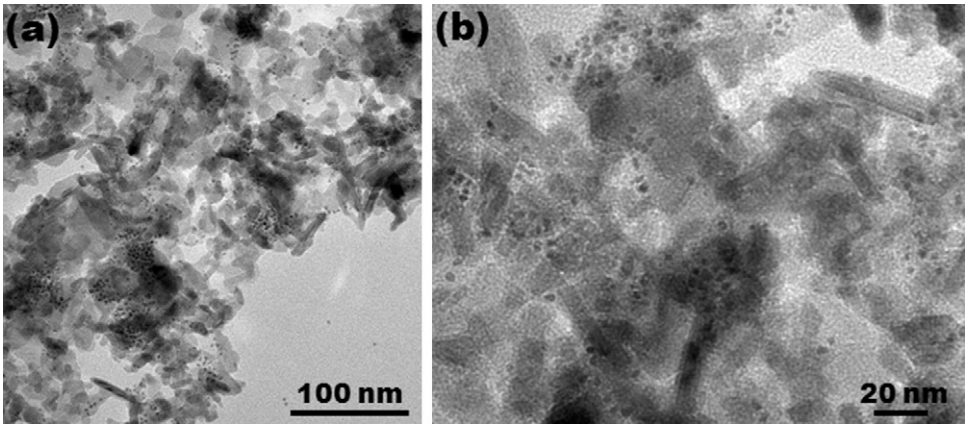

Fig. 3. (a) Low-magnification and (b) high-magnification TEM images of $Ru@Al_2O_3$.

dehydrogenation of AB in water is not possible in the colloidal form. For this reason, supporting them on a robust inorganic matrices is necessary. Nanocrystalline gamma-phase aluminum oxide (γ-Al_2O_3) has been used as a catalyst support for variety of transition metal nanoparticles [43–45]. The nanopowder form of γ-Al_2O_3 with a particle size of smaller than 50 nm and surface area larger than 40 m^2/g is commercially available nowadays and use of it as catalyst support is advantageous for the preparation of highly active heterogeneous nanocatalysts. In this regard, we used Al_2O_3 nanopowder as support matrices for Ru NPs in this study. The well-dispersed Ru NPs supported on Al_2O_3 nanopowder ($Ru@Al_2O_3$) were obtained via simple liquid impregnation method as seen from the representative TEM images of $Ru@Al_2O_3$ in Fig. 3. Ru NPs preserve their size distribution and no agglomerated particles were observable on Al_2O_3 nanopowder. The Ru content of the $Ru@Al_2O_3$ catalyst was determined as 1 wt% Ru by ICP-OES analysis performed on different catalyst samples and this value was used in the calculation of all catalyst concentration throughout the kinetic studies.

Fig. 4 shows the powder-XRD pattern of Al_2O_3 nanopowder and $Ru@Al_2O_3$ catalyst. All the peaks observed in the XRD patterns belong to γ-Al_2O_3 (JCPDS Reference No. 00-010-0425) and no peaks detected for ruthenium, probably due to the very low Ru loading or very small particle size of Ru NPs. Actually, the XRD results are consistent with the TEM image and ICP-OES analysis of $Ru@Al_2O_3$ samples, where the low loading of Ru NPs are seen and the Ru loading was determined as 1 wt% Ru, respectively.

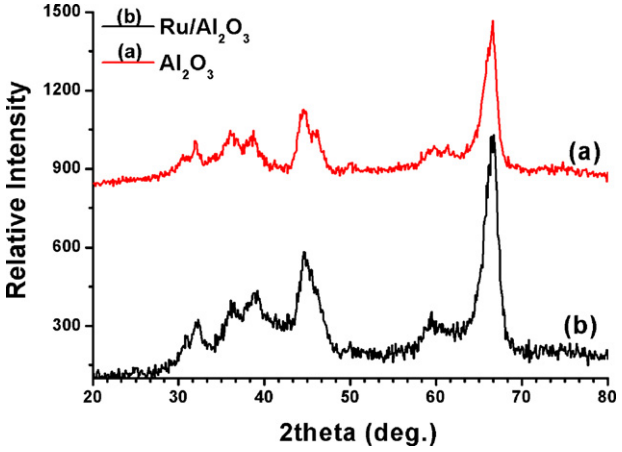

Fig. 4. Powder XRD pattern of (a) Al_2O_3 nanopowder and (b) $Ru@Al_2O_3$.

3.3. Hydrolytic dehydrogenation of AB catalyzed by $Ru@Al_2O_3$ and its detailed reaction kinetics

After the well characterization of $Ru@Al_2O_3$ catalysts, they were used as catalyst in the hydrolytic dehydrogenation of AB. They show high catalytic activity in hydrogen generation from the hydrolysis of AB without any treatment to remove surfactants. For example, in the hydrolysis of 200 mM AB catalyzed by $Ru@Al_2O_3$ ([Ru] = 1.0 mM), the initial TOF value of 39.6 mol H_2/mol Ru min was obtained by our catalysts at 25 ± 0.5 °C, which is comparable to the one of the best supported Pt catalysts (Pt/γ-Al_2O_3 with an initial TOF = 52 mol H_2/mol Pt min) [28]. Fig. 5 shows the plots of mol H_2 per mol AB versus time during the hydrolysis of AB (200 mM) in the presence of different $Ru@Al_2O_3$ concentrations (0.5–1.5 mM Ru). The hydrogen generation rate was determined from the linear portion of the plot for each catalyst concentration experiment. The hydrogen generation rate increases by increasing catalyst concentration as expected. The inset in Fig. 5 shows the plot of hydrogen generation rate versus Ru concentration, both in logarithmic scale. The line with a slope of 0.93–1.00 in the inset of Fig. 5 indicates the first order kinetics with respect to the catalyst concentration for the hydrolysis of AB in the presence of $Ru@Al_2O_3$ catalyst.

The effect of substrate concentration on the hydrogen generation rate was also studied by performing a series of experiments

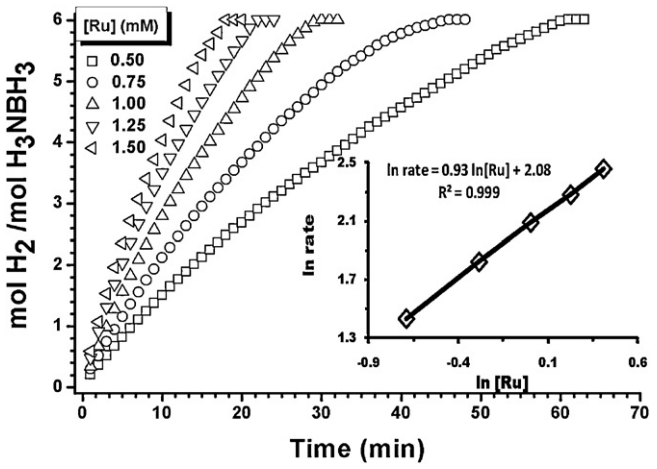

Fig. 5. The plots of mol H_2 per mol AB versus time for $Ru@Al_2O_3$ catalyzed hydrolysis of AB at different Ru concentrations ([AB] = 200 mM; T = 25 ± 0.5 °C). The inset shows the plot of hydrogen generation rate versus the concentration of Ru (both in logarithmic scale).

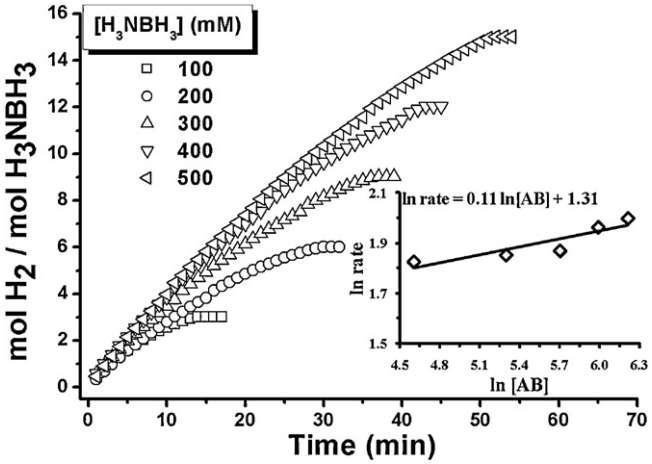

Fig. 6. The plots of the mol H_2 per mol AB versus time for $Ru@Al_2O_3$ catalyzed hydrolysis of AB at different substrate concentrations ([Ru] = 1.0 mM; $T = 25 \pm 0.5$ °C). The inset shows the plot of hydrogen generation rate versus the concentration of AB (both in logarithmic scale).

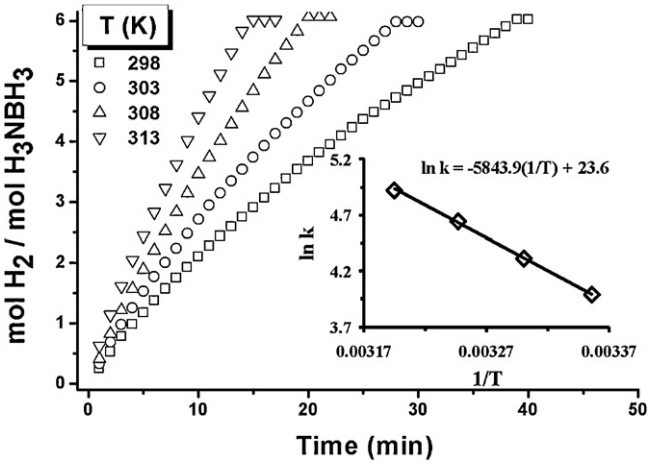

Fig. 7. The plots of the mol H_2 per mol AB versus time for $Ru@Al_2O_3$ catalyzed hydrolysis of AB at four different temperatures in the range of 298–313 K ([Ru] = 1.0 mM; [AB] = 200 mM). The inset shows the plot of hydrogen generation rate versus the concentration of AB (both in logarithmic scale).

starting with different initial concentrations of AB while keeping the catalyst concentration constant at 1.0 mM Ru at 25.0 ± 0.5 °C (Fig. 6). It can be clearly concluded by the slope of the line in the inset of Fig. 6 that the hydrogen generation rate from the catalytic hydrolysis of AB is practically independent from AB concentration. In other words, the hydrolysis of AB catalyzed by $Ru@Al_2O_3$ is zeroth order with respect to the substrate concentration. Actually, the zeroth order reaction kinetics of AB concentration is plausible considering our catalytic reaction conditions in which at least 100 fold excess AB were used compared to catalyst concentration. Thus, the rate law for the hydrolysis of AB catalyzed by $Ru@Al_2O_3$ can be given as Eq. (2):

$$\text{rate} = k^{\text{app}}[\text{Ru}] \quad (2)$$

In the final set of kinetic studies, the $Ru@Al_2O_3$ catalyzed hydrolysis of AB was carried out at various temperatures (298–313 K) in the presence of 200 mM AB and 0.75 mM Ru. Fig. 7 shows the plots of mol H_2 per mol AB versus time for the hydrolysis of AB in the presence of $Ru@Al_2O_3$ catalyst at four different temperatures. The values of apparent rate constant (k^{app}) at different temperatures were calculated by using the slope of the linear region of each plot in Fig. 7 and the rate law equation at Eq. (2). Next, they were used to draw the Arrhenius plot given in the inset of Fig. 7 to calculate the apparent activation energy: $E_a^{\text{app}} = 48 \pm 2$ kJ mol^{-1}. The apparent activation enthalpy ($\Delta H^{\#,\text{app}}$) and activation entropy ($\Delta S^{\#,\text{app}}$) for the catalytic hydrolysis of AB were also calculated to be 46 ± 2 kJ mol^{-1} and -58 ± 2 J K^{-1} mol^{-1} from the Eyring plot ($\ln(k/T)$ versus $(1/T)$), respectively.

The catalytic performance of the as-prepared $Ru@Al_2O_3$ was further enhanced by the acetic acid treatment [17]. Fig. 8a shows the mol H_2 per mol AB versus time for the hydrolysis of AB catalyzed by acetic acid-treated $Ru@Al_2O_3$. It can be clearly seen that the catalytic activity of $Ru@Al_2O_3$ catalyst is increased dramatically by acetic acid treatment. The initial TOF value of $Ru@Al_2O_3$ catalyst is increased from 39.6 to 83.3 mol H_2 (mol Ru min)$^{-1}$. In one of our recent reports, we have also reported in situ generated and colloidal Ru NPs as highly active catalyst in the hydrolysis of AB proving an initial TOF of 180 mol H_2 (mol Ru min)$^{-1}$ [14]. This value is much higher than the one reported here, but the catalyst reported there is no reusable which is very important issue on the real-life applications. In this regard, it can be said that $Ru@Al_2O_3$ is the best among reusable Ru catalysts and even higher than Pt-based catalysts tested in the hydrolysis of AB [46]. Since the $Ru@Al_2O_3$ has no morphology change after the acetic acid treatment (see TEM image in Fig. 8b), the enhanced activity is due most likely to the surface organics removal for AB hydrolysis at room temperature.

The durability of the acetic acid-treated $Ru@Al_2O_3$ in the hydrolysis of AB was studied by performing a reusability test. Fig. 9a shows the mol H_2 per mol AB versus time during the reusability test of acetic acid-treated $Ru@Al_2O_3$ (1 mM Ru) catalysts in the

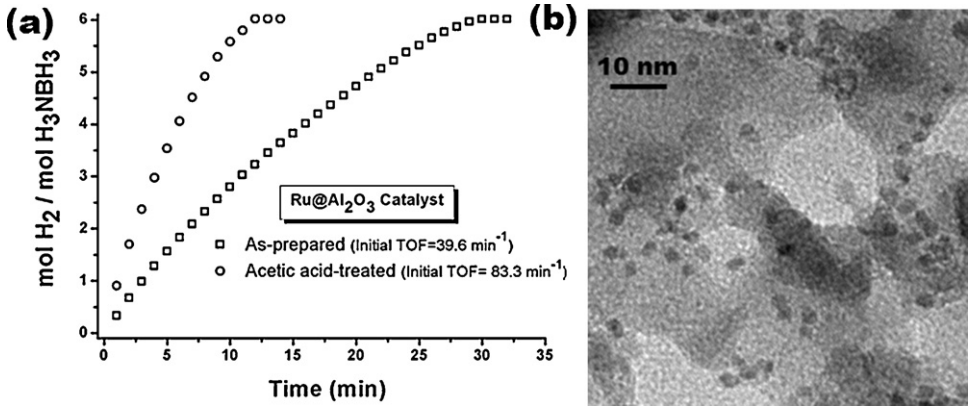

Fig. 8. (a) The plots of the mol H_2 per mol AB versus time for the hydrolysis of AB catalyzed by as-prepared and acetic acid-treated $Ru@Al_2O_3$ (1 mM Ru). (b) A representative TEM image of $Ru@Al_2O_3$ catalyst after acetic acid treatment.

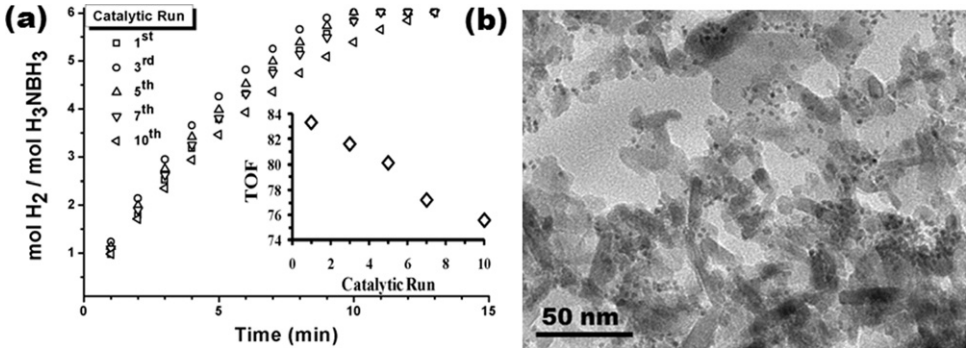

Fig. 9. (a) The plots of the mol H_2 per mol AB versus time for Ru@Al_2O_3 catalyzed hydrolysis of AB at different catalytic runs during the reusability test ([Ru] = 1.0 mM; [AB] = 200 mM; $T = 25 \pm 0.5$ °C). The inset shows the TOF values (mol H_2/(mol Ru min)) for the catalytic hydrolysis of AB at different catalytic runs. (b) A representative TEM image of Ru@Al_2O_3 catalyst after 10th run reusability test.

hydrolysis of AB (200 mM) at room temperature. The initial TOF values (mol H_2/(mol Ru min)) for each catalytic run was calculated and plotted against catalytic run given in the inset of Fig. 9. The initial TOF of Ru@Al_2O_3 catalysts decreased from 83.3 to 75.6 after 10th run, which means that they preserve 90% of their initial activity after 10th runs. Ru@Al2O3 catalyst has no significant morphology change after catalysis of 10th run as seen from the TEM image in Fig. 9b.

4. Conclusions

We have reported a unique and facile solution phase synthesis of nearly monodisperse Ru NPs that have 2.5 nm average particle size and hexagonal close packed crystal structure. As-prepared Ru NPs are very dispersible in nonpolar organic solvents such as hexane and THF. A highly active and robust heterogeneous Ru nanocatalyst was successfully generated by supporting Ru NPs on Al_2O_3 nanopowder via simple liquid impregnation method. Ru@Al_2O_3 catalysts possess high activity and excellent reusability for hydrogen generation from the hydrolytic dehydrogenation of AB under ambient conditions. The kinetic studies on the Ru@Al_2O_3 catalyzed hydrolysis of AB reveal that it is first order with respect to the catalyst concentration and zero order with respect to substrate concentration. The catalytic activity of Ru@Al_2O_3 catalyst can be further enhanced by acetic acid treatment at 70 °C in air. The activity of acetic acid-treated Ru@Al_2O_3 catalyst in terms of initial TOF value is higher than the Pt-based catalyst systems tested in the hydrolysis of AB so far. We believe that the results presented here open wide range possibilities for the application of highly active and robust heterogeneous Ru nanocatalyst in various industrial reactions.

Acknowledgments

The financial support by "Atatürk University Scientific Research Project Council (Project No: 2011/93)" is gratefully acknowledged. We would like to thank Middle East Technical University Central Laboratory and Seçkin Öztürk for TEM analyses.

References

[1] D. Astruc, Nanoparticles and Catalysis, Wiley-Interscience, New York, 2008.
[2] D. Astruc, F. Lu, J.R. Aranzaes, Angewandte Chemie-International Edition 44 (2005) 7852–7872.
[3] M. Zahmakıran, S. Özkar, Nanoscale 3 (2011) 3462–3481.
[4] J. Huang, T. Jiang, B.X. Han, W.Z. Wu, Z.M. Liu, Z.L. Xie, J.L. Zhang, Catalysis Letters 103 (2005) 59–62.
[5] A. Gual, C. Godard, S. Castillon, C. Claver, Dalton Transactions 39 (2010) 11499–11512.
[6] G. Viau, R. Brayner, L. Poul, N. Chakroune, E. Lacaze, F. Fievet-Vincent, F. Fievet, Chemistry of Materials 15 (2003) 486–494.
[7] J. Yang, J.Y. Lee, T.C. Deivaraj, H.-P. Too, Journal of Colloid and Interface Science 271 (2004) 308–312.
[8] T. Matrab, A. Yassar, G. Viau, N. Chakroune, F. Fievet, P.C. Lacaze, Journal of Colloid and Interface Science 296 (2006) 95–101.
[9] W. Chen, J.R. Davies, D. Gosh, M.C. Tog, J.P. Konopelski, S. Wie, Chemistry of Materials 18 (2006) 5253–5259.
[10] P. Lara, O. Rivada-Wheelaghan, S. Conejero, R. Poteau, K. Philippot, B. Chaudret, Angewandte Chemie-International Edition 50 (2011) 12080–12084.
[11] G.V. Chakroune, S. Ammar, L. Poul, D. Veautier, M.M. Chemini, C. Mangeney, F.N. Villain, F. Fievet, Langmuir 21 (2005) 6788–6796.
[12] T. Tsukatani, H. Fujihara, Langmuir 21 (2005) 12093–12095.
[13] C. Pan, K. Pelzer, K. Philippot, B. Chaudret, F. Dassenoy, P. Lecante, M.-J. Casanove, Journal of the American Chemical Society 123 (2001) 7584–7593.
[14] Ö. Metin, S. Sahin, S. Özkar, International Journal of Hydrogen Energy 34 (2009) 6304–6313.
[15] Z. Peng, J. Wu, H. Yang, Chemistry of Materials 22 (2010) 1098–1106.
[16] Ö. Metin, V. Mazumder, S. Özkar, S. Sun, Journal of the American Chemical Society 132 (2010) 1468–1469.
[17] V. Mazumder, S. Sun, Journal of the American Chemical Society 131 (2009) 4588–4589.
[18] B. Peng, J. Chen, Energy & Environmental Science 1 (2008) 479–483.
[19] U.B. Demirci, P. Miele, Energy & Environmental Science 2 (2009) 627–637.
[20] N.C. Smythe, J.C. Gordon, European Journal of Inorganic Chemistry 2010 (2010) 509–521.
[21] T. Umegaki, J.-M. Yan, X.-B. Zhang, H. Shioyama, N. Kuriyama, Q. Xu, International Journal of Hydrogen Energy 34 (2009) 2303–2311.
[22] U.S. Department of Energy, Office of Energy Efficiency and Renewable Energy and The FreedomCAR and Fuel Partnership, Targets for Onboard Hydrogen Storage Systems for Light-duty Vehicles, September 2009, available at: http://www1.eere.energy.gov/hydrogenandfuelcells/storage/pdfs/targets_onboard_hydro_storage_explanation.pdf.
[23] T.B. Marder, Angewandte Chemie-International Edition 46 (2007) 8116–8118.
[24] F.H. Stephens, V. Pons, R.T. Baker, Dalton Transactions 25 (2007) 2613–2626.
[25] C.W. Hamilton, R.T. Baker, A. Staubitz, I. Manners, Chemical Society Reviews 38 (2009) 279–293.
[26] A. Staubitz, A.P.M. Robertson, I. Manners, Chemical Reviews 110 (2010) 4079–4124.
[27] H.L. Jiang, S.K. Singh, J.M. Yan, X.B. Zhang, Q. Xu, ChemSusChem 3 (2010) 541–549.
[28] Q. Xu, M. Chandra, Journal of Alloys and Compounds 446–447 (2007) 729–732.
[29] Ö. Metin, S. Özkar, Energy & Fuels 23 (2009) 3517–3526.
[30] N. Patel, A. Kale, A. Miotello, Applied Catalysis B 111–112 (2012) 178–184.
[31] B.L. Davis, D.A. Dixon, E.B. Garner, J.C. Gordon, M.H. Matus, B. Scott, F.H. Stephens, Angewandte Chemie-International Edition 48 (2009) 6812–6816.
[32] H.L. Jiang, Q. Xu, Catalysis Today 170 (2011) 56–63.
[33] M. Rakap, S. Özkar, International Journal of Hydrogen Energy 36 (2011) 7019–7027.
[34] M. Rakap, S. Özkar, International Journal of Hydrogen Energy 35 (2010) 1305–1312.
[35] J.-M. Yan, X.-B. Zhang, T. Akita, M. Haruta, Q. Xu, Journal of the American Chemical Society 132 (2010) 5326–5327.
[36] Ö. Metin, S. Özkar, S. Sun, Nano Research 3 (2010) 676–684.
[37] M. Rakap, S. Özkar, Applied Catalysis B 91 (2009) 21–29.
[38] Ö. Metin, M. Dinç, Z.S. Eren, S. Özkar, International Journal of Hydrogen Energy 36 (2011) 11528–11535.
[39] C.A. Jaska, K. Temple, A.J. Lough, I. Manners, Chemical Communications 11 (2001) 962–963.

[40] M. Chandra, Q. Xu, Journal of Power Sources 168 (2007) 135–142.
[41] P.-Z. Li, K. Aranishi, Q. Xu, Chemical Communications 48 (2012) 3173–3175.
[42] P.G. Rachiero, U.B. Demirci, P. Miele, Catalysis Today 170 (2011) 85–92.
[43] F. Su, L.v. Lu, F.Y. Lee, T. Liu, A.I. Cooper, X.S. Zhao, Journal of the American Chemical Society 129 (2007) 14213–14223.
[44] L. Zhang, C. Zhang, H. He, Journal of Catalysis 261 (2009) 101–109.
[45] L. Xu, C. He, M. Zhu, S. Fang, Catalysis Letters 114 (2007) 202–205.
[46] D. Sun, V. Mazumder, Ö. Metin, S. Sun, ACS Nano 8 (2011) 6458–6464 (please see the Table 1 for the TOF values of various catalyst systems reported in the hydrolysis of AB).